American Mineralogist, Volume 93, pages 667–675, 2008

Synchrotron powder X-ray diffraction study of the structure and dehydration behavior of palygorskite

JEFFREY E. POST[1,*] AND PETER J. HEANEY[2]

[1]Department of Mineral Sciences, Smithsonian Institution, Washington, D.C. 20560-0119, U.S.A.
[2]Department of Geosciences, Pennsylvania State University, University Park, Pennsylvania 16802, U.S.A.

ABSTRACT

Rietveld refinements using synchrotron powder X-ray diffraction data were used to study the crystal structure and dehydration behavior of pure monoclinic palygorskite samples from Korea and Alaska. The 300 and 100 K palygorskite structures in air compare well with previous models but provide additional details about zeolitic H_2O sites and reveal that the Al atoms are ordered into the inner M2 octahedral sites and the Mg cations into the M3 sites at the edges of the tunnels. Real-time, temperature-resolved synchrotron powder X-ray diffraction data and Rietveld refinements were used to investigate the monoclinic palygorskite structure from 300 to 1400 K (in air). Rietveld refinements showed that most of the zeolitic H_2O is lost by ~425 K, accompanied by a decrease in the unit-cell volume of 1.3%, primarily owing to a decrease in the *a* unit-cell parameter and an increase in the β angle. The structurally bound H_2O is lost in two stages, at temperature intervals of 475–540 and 580–725 K. Above ~825 K in air a portion of the Korean sample transformed to a folded structure; the Alaskan sample folded at ~575 K under vacuum. A structure model was refined for the folded structure. At ~1015 K for the sample heated in air, β-quartz diffraction peaks appeared and increased in intensity as heating continued to the maximum temperature. Cristobalite formed above ~1050 K, along with a small amount of clinoenstatite, and both phases persisted to the maximum temperature studied.

Keywords: Palygorskite, Rietveld, synchrotron, X-ray diffraction, time-resolved

INTRODUCTION

Palygorskite is a hydrous Mg- and Al-rich silicate clay mineral with a fibrous morphology that typically occurs as fine-grained, poorly crystalline masses. It is found in a wide variety of geological environments, commonly as felted masses or sheets, referred to as mountain cork or mountain leather (Heddle 1878), respectively. The term "attapulgite" was applied by De Lapparent (1935) to a clay mineral encountered in Fuller's Earth from Attapulgus, Georgia, but Stephan (1954) and others determined that it was identical to palygorskite, and recommended that the term "attapulgite" be discontinued. Palygorskite has been mined for centuries because of its many useful properties and boasts more than 100 commercial uses today in the pharmaceutical, fertilizer, and pesticide industries (Van Scoyoc et al. 1979; Jones and Galan 1988; Galan 1996), and its versatile functionality derives from the large surface area and microporosity that are characteristic of the material. In recent years, palygorskite has received considerable attention with regard to the adsorption of organics and for use as a support for catalysts (Jones and Galan 1988). Historically, palygorskite was the predominant clay component that, when combined with indigo, produced the vibrant Maya blue pigment (e.g., José-Yacamán et al. 1996).

Palygorskite has a layer structure constructed of ribbons of 2:1 phyllosilicate modules comprised of linked double silicate chains that sandwich Mg,Al-(O,OH) octahedral strips (Fig. 1). The ribbons are connected via Si-O-Si bonds between SiO_4 tetrahedra that are inverted relative to each other. Palygorskite has continuous tetrahedral sheets, but with tetrahedral apices pointing in opposite directions in adjacent ribbons. Unlike other phyllosilicates, it lacks continuous octahedral sheets. The structure has large tunnels parallel to the phyllosilicate ribbons that are partially occupied by H_2O molecules. The tunnels measure 3.7 × 6.0 Å in cross section.

The palygorskite structure was deduced by Bradley (1940) from fiber X-ray diffraction (XRD) patterns, and his model is monoclinic with space group *C2/m*. This structural scheme was affirmed by Drits and Sokolova (1971). Christ et al. (1969) analyzed powder XRD data for five palygorskite samples and concluded that palygorskite exists in structurally related orthorhombic and monoclinic forms. Chisholm (1992) compared observed and theoretical powder XRD patterns and noted that most palygorskite samples are mixtures of monoclinic and orthorhombic polymorphs.

Galan and Carretero (1999) reviewed chemical analyses from the literature and concluded that palygorskite is intermediate between dioctahedral and trioctahedral with a formula close to $(Mg_2R^{3+}_2\square_1)(Si_{8-x}Al_x)O_{20}(OH)_2 \cdot R^{2+}_{x/2}(H_2O)_4$, where □ = vacancy, R = primarily Al^{3+}, Fe^{3+}, Fe^{2+}, and Mn^{2+}, and x = 0–0.5. The octahedral sheet has four of five sites occupied, and $Mg^{2+}/(Al^{3+}$ +

* E-mail: postj@si.edu

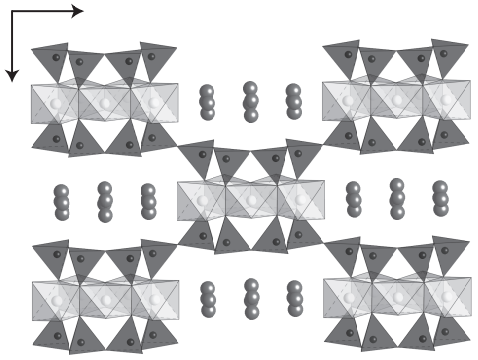

FIGURE 1. Polyhedral crystal structure representations, viewed approximately along *c*, resulting from the Rietveld refinements for palygorskite at 300 K in air. Shaded circles represent zeolitic H_2O molecules.

Fe^{3+}) is close to 1.0. They observed that the degree of tetrahedral substitution is low, <0.5 atoms of ($Al + Fe^{3+}$), and the number of octahedral Mg atoms ranges from 0.87 to 1.56, and octahedral ($Al + Fe^{3+}$) from 0.82 to 1.45.

Because it is fine-grained and poorly crystalline, it has not been possible to study the crystal structure of palygorskite using single-crystal diffraction methods, and consequently many details of the structure are not known. Recently, Rietveld refinements using powder X-ray and neutron diffraction data confirmed the basic monoclinic and orthorhombic palygorskite structure models. Artioli et al. (1994) used theoretical structures developed by Chisholm (1992) to model the powder XRD pattern for a mixed orthorhombic and monoclinic palygorskite sample. Chiari et al. (2003) investigated the structure of Maya Blue (palygorskite with indigo molecules in the tunnels) using the Rietveld method and synchrotron powder XRD data. The most complete structural study to date is by Giustetto and Chiari (2004) who carried out a Rietveld refinement for a deuterated, mixed monoclinic and orthorhombic palygorskite sample using powder neutron diffraction data.

Each of the structure refinements mentioned above used palygorskite samples that were mixtures of monoclinic and orthorhombic polymorphs, as is the case for most natural palygorskite samples (Chisholm 1992). Although each study provided significant new information, the refinements were challenged by the difficulty of simultaneously refining two similar structures from severely overlapping powder diffraction patterns. In the current study, we examined by powder XRD more than 30 palygorskite samples from the Smithsonian Institution's National Museum of Natural History mineral collection, and identified two samples that yielded nearly identical diffraction patterns that matched well the theoretical pattern for monoclinic palygorskite reported by Chisholm (1992). Subsequent Rietveld refinements confirmed that the samples are the monoclinic polymorph with no orthorhombic component. In this study, we used synchrotron powder X-ray diffraction data and Rietveld refinements to better characterize the structure and dehydration of monoclinic palygorskite. We refined room-temperature (300 K) structures for two palygorskite samples and a structure using data collected at 100 K.

In the second part of our study, we used temperature-resolved real-time synchrotron powder XRD and Rietveld analysis to investigate in detail changes in the monoclinic palygorskite structure as it dehydrated from 300 to 1400 K. The Bradley (1940) structure model includes three types of H_2O: zeolitic H_2O molecules in the tunnels, crystallographically bound H_2O molecules that complete the coordination of the Mg atoms at the edges of the octahedral strips, and hydroxyl (OH) groups bonded to some of the Mg and Al atoms. Numerous studies have monitored the dehydration of palygorskite using thermogravimetric analysis (TGA) and differential thermal analysis (DTA) methods (e.g., Stephen 1954; Kulbicki 1959; Preisinger 1963; Hayashi et al. 1969; Tien 1973; Serna et al. 1977; Van Scoyoc et al. 1979; Artioli et al. 1994; Kuang et al. 2004; Giustetto and Chiari 2004). The samples used for these studies were almost certainly mixtures of monoclinic and orthorhombic palygorskite, and therefore the reported thermal behaviors represent weighted averages for the two polymorphs, which might explain some of the variations observed. There is, however, a general concurrence that zeolitic H_2O is lost during heating from RT to ~450 K, bound H_2O molecules are released in two stages between ~475 and 875 K; and hydroxyl groups are lost above ~900 K. Preisinger (1963) proposed that loss of the bound H_2O causes a phase change during which the structure folds by rotation of the phyllosilicate ribbons about an axis through the Si-O-Si bonds that link the ribbons (Fig. 2). Rautureau and Mifsud (1977) show high-resolution transmission electron microscope images that appear to confirm the existence of a folded "anhydrous" structure for the closely related phase sepiolite, and recently Post et al. (2007) completed a structure refinement for folded sepiolite. Our results confirm the basic Preisinger (1963) folded-structure model for palygorskite.

The many thermal analysis studies listed above provide a generally consistent description of the dehydration behavior of palygorskite. It is not always straightforward, however, to relate specific structural changes to features in TGA or DTA curves, leaving room for multiple and sometimes conflicting interpretations of these data. We present here the results of a series of refinements of the palygorskite structure over the temperature range 300 to ~825 K that provide, for the first time, a direct look at changes in the palygorskite structure with increasing temperature as it undergoes dehydration and decomposition.

DATA COLLECTION AND REFINEMENT

The palygorskite samples used for this study, NMNH 117101 and NMNH R12180 are from Lemesurier Island, Alaska and Yulu River, Korea, respectively, and powder X-ray diffraction data revealed that they are exceptionally well ordered for palygorskite. Powder XRD detected a small amount of halite in the Alaskan sample. For electron microprobe analyses (EMPA) (JEOL JXA-8900R), one set of samples was embedded in epoxy, polished, and carbon-coated, and a second was pressed flat using a pellet press designed for preparing samples for infrared spectroscopy and carbon-coated. EMPA yielded the following formulae: Alaska = $(Mg_{1.97}Al_{2.02}Fe^{3+}_{0.09}\square_{0.92})(Si_{7.82}Al_{0.18})O_{20}(OH)_2{\cdot}(Ca_{0.01}K_{0.01})(H_2O)_4$, and Korea = $(Mg_{2.09}Al_{1.92}Fe^{3+}_{0.11}\square_{0.88})(Si_{7.80}Al_{0.20})O_{20}(OH)_2{\cdot}(Ca_{0.01}Na_{0.01})(H_2O)_4$. The embedded samples yielded analytic totals of 60 to 70 wt%, whereas analyses of the pressed samples summed to 80–85 wt%, with an average total of ~82 wt%. The water by difference from the pressed samples, ~18 wt%, is close to the value of ~20 wt% calculated from the above structural formulae for total zeolitic, structural, and hydroxyl H_2O. The samples used for X-ray diffraction were hand ground under acetone in an agate mortar and passed through a 325-mesh sieve. Samples were loaded into 0.7 and 0.5 mm quartz-glass capillaries for the 100 K, room-temperature (300 K), and heating synchrotron XRD studies. XRD data were collected at beam line X7B of the National Synchrotron Light Source (NSLS), Brookhaven National

Laboratory (BNL), using wavelengths of 0.9492 (300 K), 0.9218 (100 K), and 0.9274 Å (heating experiment) and a MAR345 full imaging plate detector. Diffraction data used for the palygorskite structure refinements were collected at 300 and 100 K using 120 s exposures from samples in air. The sample for the 100 K experiment was cooled with a cold air stream from a liquid N_2 cryostat using an Oxford Cryostream 600 series controller.

The heating experiment was performed in air using a Blake Instruments furnace with a Pt-13%Rh coiled wire yoke encased in ZrO_2 cement (Brown et al. 1973). The temperature was varied with an Omega controller and monitored with a Chromel-Alumel thermocouple located ~2 mm from the specimen. The actual sample temperature was determined for the range 298 to 1273 K by a variety of phase and melting transitions and by the placement of an additional thermocouple in the sample position. The highly linear relationship between the observed and actual temperatures ($r^2 = 0.983$) allowed us to calculate a calibration curve with an estimated error of ±5 K for a given temperature. Temperature-resolved data from 300 to 1335 K were collected as a series of 120 s exposures with a MAR345 full imaging-plate detector. The temperature was increased continuously at 3.0 K/min and measurements were obtained every ~11.5 K, owing to down time for repositioning of the sample and reading the imaging plate; thus, each exposure encompassed a temperature range of ~6.0 K. During each exposure the sample was rotated through a 120° angle. Preferred orientation of the powder was eliminated through a combination of the specimen rotation, use of a capillary sample holder, and full intensity integration of the diffraction rings, as obtained using the program Fit2D (Hammersley et al. 1996) with a polarization factor of 0.93.

Rietveld refinements were performed using the general structure analysis system (GSAS) of Larson and Von Dreele (2007) using data sets measured at 100 K in air, at 300 K in air, and at selected temperatures when heated in air to the point at which the structure folded (~825 K). The starting structural parameters for the monoclinic palygorskite phyllosilicate modules were taken from Chisholm (1992). The model for the folded "anhydrous" palygorskite was derived graphically from a model illustrated in Preisinger (1963), and Mg-O and Si-O bond distances were optimized in a monoclinic unit cell ($P2_1/a$) using the GSAS bond distance constraint feature with a large weighting factor (F = 5000). Initially, the Si-O distances were constrained to 1.61 Å (sigma of 0.02), and for the folded structure the Mg,Al-O distances also were constrained to 2.03 Å (sigma of 0.04). The diffraction pattern backgrounds were fit using a linear interpolation function. Peak profiles were modeled by a pseudo-Voigt profile function as parameterized by Thompson et al. (1987) with asymmetry corrections by Finger et al. (1994) and microstrain anisotropic broadening terms by Stephens (1999). Displacement factors for a given atom type were constrained to be equivalent.

During the initial cycles of refinement, only the background, scale, peak profile, and unit-cell parameters were allowed to vary. After convergence, difference-Fourier maps were calculated to locate the O atoms of the H_2O molecules in the tunnels. These O atoms were added to the model and all atom positions, displacement factors, and occupancy factors of the O atoms of the H_2O molecules were refined. Soft constraints were used to limit the Si-O bond distances to within the range observed in similar silicate structures, e.g., tuperssuatsiaite (1.58–1.63 Å, <1.61 Å>; Cámara et al. 2002) and raite (1.59–1.65 Å, <1.62 Å>; Pluth et al. 1997). The weighting factors for the constraints were gradually reduced. Attempts to eliminate the weighting factors resulted in Si-O distances of 1.55 (Si2-O3) and 1.77 Å (Si1-O2), and therefore the smallest weighting factor (F = 10) that yielded reasonable Si-O distances (i.e., 1.58–1.65 Å) was retained. The bond constraint χ^2 contribution accounted for 106 out of a total χ^2 contribution of 5987. For folded palygorskite, the Si-O and Mg-O distances were constrained throughout the refinement (F = 50).

The final refinement parameters for 300 K palygorskite in air (Korea and Alaska) and at 100 K (Korea) and results for folded palygorskite (Alaska) are listed in Table 1. The refined atom positions for the samples in air for the Korean and Alaskan samples and for the Korean sample at 100 K are not significantly different; therefore, the complete set of atom positions is given in Table 2 for the Korean sample in air. (The full set of atom positions for palygorskite at 100 K is listed in Appendix 1.[1]) Refined framework atom positions for folded palygorskite were similar at all temperatures and therefore only the values determined at 1160 K are reported in Table 3. Selected bond distances for 300 K palygorskite in air are reported in Table 4. The final observed, calculated, and difference patterns for the 300 K palygorskite sample in air and folded palygorskite (1160 K) are plotted in Figures 3 and 4, respectively. The standard deviations calculated by GSAS for the lattice parameters are likely lower than the true errors (Post and Bish 1989).

Results and discussion

Palygorskite at 300 K in air

In general, the refined monoclinic palygorskite model determined using the XRD data collected at 300 K in air from both samples (Fig. 1) compare well with the Bradley (1940) model as parameterized by Chisholm (1992) and to recent refinements by Chiari et al. (2003) and Giustetto and Chiari (2004). In addition to minor differences for some atom positions, we did not locate the ZW3 zeolitic H_2O site reported by Giustetto and Chiari (2004).

The unit-cell parameters for the Alaska and Korea samples at 300 K are nearly the same (Table 1); the slightly smaller unit cell of the Alaskan palygorskite and larger β angle might reflect

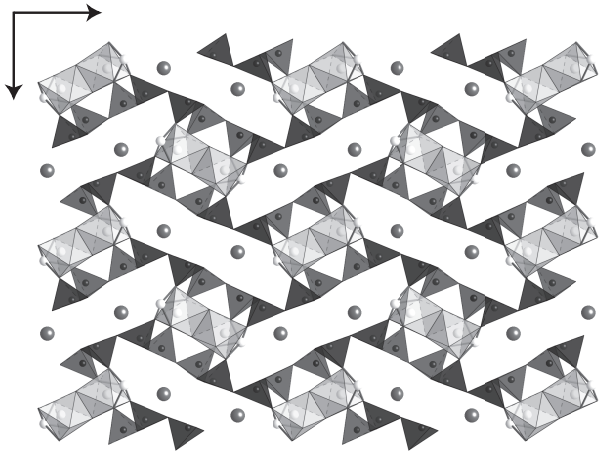

Figure 2. Folded structure resulting from the Rietveld refinement for the Alaskan palygorskite heated in vacuum (1160 K) viewed along the monoclinic *c* axis.

[1] Deposit Item AM-08-018, Appendix 1. Deposit items are available two ways: For paper copy contact the Business Office of the Mineralogical Society of America (see inside cover of recent issue) for price information. For an electronic copy visit the MSA web site at http://www.minsocam.org, go to the American Mineralogist Contents, find the table of contents for the specific volume/issue wanted, and then click on the deposit link there.

Table 1. Final Rietveld refinement parameters for palygorskite in air and under vacuum

	Korea		Alaska	
	300 K	100 K	300 K	1160 K (folded)*
Space group	*C2/m*	*C2/m*	*C2/m*	$P2_1/a$
Unit cell				
a (Å)	13.2858(8)	13.179(1)	13.282(2)	10.755(2)
b (Å)	17.8476(7)	17.852(2)	17.832(1)	15.353(3)
c (Å)	5.2419(2)	5.2316(4)	5.2400(3)	5.281(9)
β (°)	107.560(5)	107.77(1)	107.66(1)	96.17(5)
V (Å^3)	1185.0(1)	1172.2(2)	1182.5(2)	867(1)
Refinement				
No. of data points	1923	1640	2185	2199
No. of reflections	466	527	750	820
Diffraction range (d Å)	1.18–6.84	1.102–8.04	1.13–8.90	1.18–13.4
No. of variables	75	74	85	83
R (F^2)	0.019	0.037	0.052	0.009
R_{wp}	0.022	0.014	0.020	0.015
χ^2	3.04	2.20	4.91	2.00

* Under vacuum.

TABLE 2. Atomic coordinates and isotropic displacement factors for 300 K palygorskite (Korea)

Atom	x	y	z	Site occupancy factor	U_{iso} (Å^2)*
M1	0	0.0804(4)	0.5	1.0	0.005(2)
M2	0	0.1681(4)	0	1.0	0.005(2)
M3	0	0	0	0.14(1)	0.005(2)
Si1	0.2140(4)	0.0845(2)	0.972(1)	1.0	0.01 (1)
Si2	0.2081(4)	0.1640(2)	0.476(1)	1.0	0.01 (1)
O1	0.0667(9)	0	0.413(3)	1.0	0.01 (1)
O2	0.0838(7)	0.0883(4)	0.853(2)	1.0	0.01 (1)
O3	0.0800(7)	0.1586(4)	0.388(2)	1.0	0.01(1)
O4	0.1027(6)	0.2528(4)	0.916(2)	1.0	0.01(1)
O5	0.25	0.25	0.5	1.0	0.01(1)
O6	0.252(1)	0	0.004(2)	1.0	0.01(1)
O7	0.2570(8)	0.1264(7)	0.260(2)	1.0	0.01(1)
O8	0.2661(8)	0.1232(5)	0.761(2)	1.0	0.01(1)
OW1	0.450(1)	0	0.697(3)	1.08(2)	0.12(1)
OW2	0.472(1)	0.1487(6)	0.551(3)	0.58(1)	0.05(1)
H	0.13 (1)	0	0.42(4)	0.7(2)	0.015

* Isotropic displacement factors for same atom types were constrained to be equal.

TABLE 3. Atomic coordinates and isotropic displacement factors for folded palygorskite (Alaska) at 1160 K in vacuum

Atom	x	y	z	Site occupancy factor	U_{iso} (Å^2)*
Mg1	0.938(1)	0.101(1)	0.486(4)	1.0	0.015
Mg2	0.882(2)	0.172(1)	0.916(5)	1.0	0.015
Si1	0.154(1)	0.168(1)	0.850(4)	1.0	0.015
Si2	0.093(1)	0.262(1)	0.321(4)	1.0	0.015
O1	0.084(2)	0.036(2)	0.439(6)	0.1(1)	0.015
O2	0.017(2)	0.128(1)	0.800(5)	1.0	0.015
O3	0.976(2)	0.196(1)	0.276(5)	1.0	0.015
O9	0.565(2)	0.841(2)	0.786(9)	1.0	0.015
O5	0.076(2)	0.360(1)	0.417(7)	1.0	0.015
O6	0.244(2)	0.106(1)	0.013(4)	1.0	0.015
O7	0.147(2)	0.252(1)	0.044(5)	1.0	0.015
O8	0.161(3)	0.225(3)	0.590(6)	0.30(3)	0.015
Si1b	0.247(1)	0.506(1)	0.089(4)	1.0	0.015
Si2b	0.142(1)	0.447(1)	0.552(4)	1.0	0.015
O2b	0.856(2)	0.064(1)	0.150(5)	1.0	0.015
O3b	0.778(2)	0.107(2)	0.604(6)	1.0	0.015
O7b	0.639(2)	0.017(2)	0.840(4)	1.0	0.015
O8b	0.659(2)	0.985(1)	0.327(4)	1.0	0.015

* Isotropic displacement factors were fixed to typical values for silicate structures.

TABLE 4. Selected bond distances (Å) for palygorskite in air at RT

Al-O1	1.82(1) ×2	Mg-O2	2.09(1) ×2
Al-O2	1.85(1) ×2	Mg-O3	2.00(1) ×2
Al-O3	1.95 (1) ×2	Mg-O4	2.17(1) ×2
<Al-O>	1.87	<Mg-O>	2.09
M1-O1	2.08(1) ×2		
M1-O2	2.20(1) ×4		
<M-O>	2.16		
Si1-O2	1.655(8)	Si2-O3	1.626(8)
Si1-O6	1.581(5)	Si2-O5	1.625(4)
Si1-O7	1.626(8)	Si2-O7	1.613(8)
Si1-O8	1.626(8)	Si2-O8	1.629(8)
<Si1-O>	1.62	<Si2-O>	1.62
OW1-OW1	2.78(3)	OW2-O4	2.79(1)
OW1-OW1′	3.05(3)	OW2-O4′	2.93(2)
OW1-OW2	2.80(1)	OW2-O7	2.83(2)
		OW2-OW2	1.03(3)

Note: Soft constraints were applied to Si-O distances (see text) during refinement. Al is on the M2 and Mg on the M3 site.

its greater Al/Mg value compared to the Korean sample. The β angles are close to the value of 107° reported for monoclinic palygorskite by Drits and Sokolova (1971), but are larger than the value of 105.20° determined by Chisholm (1992) for an idealized monoclinic structure in which the chains of tetrahedra on either side of the octahedral strip are displaced relative to each other

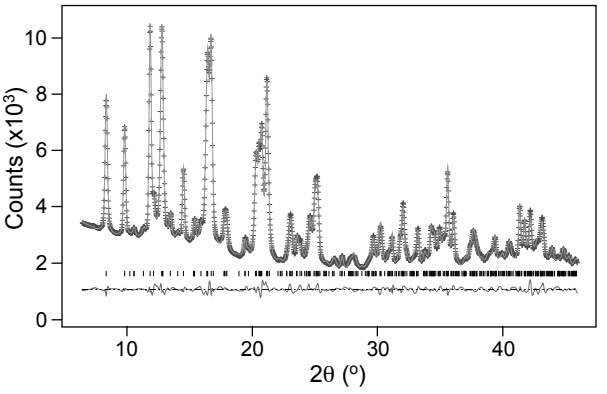

FIGURE 3. Final observed (crosses), calculated (solid line), and difference (lower) patterns for the Rietveld refinement for palygorskite (Korea) in air using the 300 K synchrotron powder X-ray diffraction data.

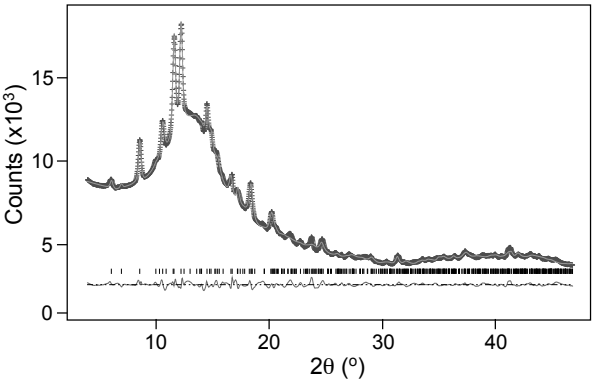

FIGURE 4. Final observed (crosses), calculated (solid line), and difference (lower) patterns for the Rietveld refinement for folded palygorskite (Alaska) in vacuum using synchrotron powder X-ray diffraction data collected at ~1160 K.

by c/3, resulting in almost regular octahedral sites. Our β angles indicate displacements close to 0.38c, which is similar to values for many monoclinic amphiboles and pyroxenes (Chisholm 1992), and is consistent with the distorted octahedral sites in our refined structures (Table 4). Our results also fall close to the β-angle values of 107.01 and 105.27° determined for a Mexican palygorskite sample (mixed orthorhombic and monoclinic phases) by Rietveld refinement using synchrotron X-ray (Chiari et al. 2003) and neutron (Giustetto and Chiari 2004) diffraction data, respectively.

In contrast to other published Rietveld structure refinements of palygorskite, we did not apply soft constraints to the (Mg/Al)-O distances. The bond distances for the M2 octahedral site are significantly smaller than those for the M3 site, even considering experimental error. The refined M-O distances for M2 range from 1.82 to 1.95 Å (Table 4) with a mean of 1.87 Å, and those for M3 range from 2.00 to 2.17 Å with a mean value of 2.09 Å. The mean M-O distance for M2 is close to the ideal value of 1.89 Å for Al-O in octahedral coordination (Shannon 1976), and the mean M-O distance for M3 is near the ideal value of 2.08 Å (Shannon 1976) for Mg-O in octahedral coordination, suggesting that the M2 site is occupied by Al and the M3 site is filled

with Mg. This result is consistent with the microprobe analyses that yielded a formula with approximately equal amounts of octahedral Mg and Al (Mg/Al = 0.99 for the Korean sample). Furthermore, Serna et al. (1977) concluded from IR spectra for palygorskite from Attapulgus, Georgia that Mg cations occur at the edge of the channels near the coordinated H_2O molecules. Similarly Heller-Kallai and Rozenson (1981) concluded from Mössbauer and IR spectroscopy that Fe cations and Mg preferentially occupy the M3 site, and Corma et al. (1990) observed that acid extraction experiments removed cations from palygorskite in the order: Mg > Fe > Al, suggesting that Mg was on the more accessible M3 site.

In the Bradley (1940) palygorskite model, four out of five sites in the octahedral strips contain cations, and the M1 site at (0, 0, 0) is vacant. This model is consistent with chemical analyses of pure palygorskite samples from four different localities by Smith and Norem (1986) that yielded an average of 3.97 cations and 1.03 vacancies on the octahedral sites (per 21 O atoms), and it agrees with results from Rietveld refinements by Artioli et al. (1994), Chiari et al. (2003), and Giustetto and Chiari (2004). The octahedral cation totals (Mg + Fe +Al) for the two palygorskite samples used here are 4.08 for the Alaskan sample and 4.12 for the Korean specimen. If the analyses are accurate, the excess cations are accommodated in two possible places in the structure: (1) in the supposedly vacant M1 octahedral site, or (2) in the tunnels. Our refinements at 300 K showed small occupancy factors [0.10 (Alaska) and 0.12 (Korea) Mg atoms] for M1, and these are comparable to the excesses observed by EMPA. The structures for raite (Pluth et al. 1997) and tuperssuatsiaite (Cámara et al. 2002), which are isostructural with palygorskite, have fully occupied octahedral strips. As discussed below, however, our refinements do not rule out the possibility that excess cations reside within the tunnels.

As discussed above, the Si-O distances were softly constrained during the refinement, and all fall in the range of 1.58–1.65 Å (Table 4). The microprobe analyses indicate that the contents of the tetrahedral sites are Alaska = $(Si_{7.82}Al_{0.18})$ and Korea = $(Si_{7.80}Al_{0.20})$. The small amounts of Al on the tetrahedral sites is consistent with a review of palygorskite analyses by Galan and Carretero (1999), who concluded that a maximum of 0.5 Al cations per 8 Si cations can occupy the tetrahedral sites. Also, nuclear magnetic resonance ^{27}Al spectra for palygorskite (Güven et al. 1992) indicated that Al predominantly was in octahedral coordination, and Al tetrahedral substitution was negligible.

The palygorskite model of Bradley (1940) contains three hydrous species: OH^- anions at the O1 site, coordinated to M1 (if occupied) and M2; structural H_2O at the O4 site, where it completes the M3 coordination at the edges of the Mg/Al-(O, OH, H_2O) octahedral strips; and two zeolitic H_2O positions in the tunnels. We assumed that O1 is OH^- and O4 is structural H_2O. The refined occupancy factor for the O4 site indicated that it is fully occupied at 300 and 100 K.

Difference-Fourier maps and subsequent Rietveld refinement revealed two zeolitic H_2O sites, close to those of the Bradley (1940) model. Refined occupancy factors indicated that the OW1 and OW2 sites are full, or nearly so, giving a total of ~4 zeolitic H_2O molecules per 8 tetrahedra, in agreement with most palygorskite formulae as determined by chemical or thermogravimetric analyses (e.g., Preisinger 1963; Hayashi et al. 1969; Tien 1973; Jones and Galan 1988) and to our electron microprobe analyses. Our two refined zeolitic H_2O positions compare well to those determined in a molecular modeling study of palygorskite by Fois et al. (2003). Giustetto and Chiari (2004) collected powder neutron diffraction data from a deuterated sample and used Rietveld analysis to model zeolitic H_2O positions in the monoclinic and orthorhombic palygorskite. They describe disordered arrangements of zeolitic H_2O molecules that are different for the two polymorphs. Two of these positions in their monoclinic model are similar to those determined here, but we did not find their third zeolitic H_2O site (ZW3). Our attempts to add an O atom at the ZW3 position yielded refined occupancy factors of zero for the Korean and Alaskan samples. Giustetto and Chiari (2004) reported a total occupancy for their three zeolitic H_2O sites of 4.78 per eight tetrahedra, which is higher than most reported values, but is close to some. The fact that we did not find a third zeolitic water site might reflect the compositional variation of palygorskite samples or the limitations of our respective refinements.

The interatomic distances among the zeolitic H_2O(O) sites range from 2.78 to 3.05 Å (Table 4) and are typical for H-bonded distances. The OW2-OW2 distance of 1.03 Å indicates that H_2O molecules cannot occupy adjacent OW2 sites, as is consistent with the refined occupancy factor of ~0.5. Initially, the refinement indicated split OW1 positions, separated by ~0.1 Å, but an equally good result was obtained with a single site on the mirror plane. The large refined displacement factor (U = 0.12) for OW1, however, suggests positional disorder. OW2 is the only zeolitic H_2O molecule within reasonable H-bonded distances, 2.79 and 2.93 Å, of the structural H_2O (O4); OW2 is 2.83 Å from O7 and is the only zeolitic H_2O molecule close to a framework O atom. These results are similar to those of Giustetto and Chiari (2004), who determined that the structural H_2O (O4) in palygorskite forms apparent H-bonds with zeolitic H_2O molecules, at distances of ~2.55 and 2.85 Å. Thus, although the zeolitic H_2O molecules in palygorskite exhibit a reasonable degree of H-bonding among themselves, they are not strongly linked to the surrounding structural framework, particularly OW1, perhaps explaining why they are easily lost when palygorskite is exposed to vacuum or to gentle heating.

Although conventional wisdom suggests that locating H atom positions in minerals using powder XRD data is largely a futile exercise, it is interesting that the difference Fourier map for the Korean palygorskite sample showed a weak but distinct electron density peak near the O1 atom at a position expected for a hydroxyl H atom. After adding the zeolitic H_2O(O) atoms into the model, we placed an H atom as indicated by the difference map. The refinement yielded an occupancy factor of ~0.7 and an O1-H distance of 0.8 Å, which is short for an O-H bond, but typical for such distances, refined using XRD data. The refined H position shows an O1-H bond oriented perpendicular to the structural sheets, and the H atoms are located in the centers of the tetrahedral rings, as is consistent with observations in similar structures and predictions from spectroscopy studies (Serna et al. 1977). If this result is not an artifact of the Rietveld refinement, it does suggest that for light-element structures, like palygorskite, positionally ordered H atom positions (such as

those associated with OH anions) might be discerned in electron difference syntheses.

100 K structure

The structure refinement using data collected at 100 K was carried out primarily to obtain better defined zeolitic H_2O sites. The results, however, were not significantly different from the 300 K structure, indicating that the large refined displacement factors for these positions probably are manifestations of positional rather than dynamic disorder. Giustetto and Chiari (2004) similarly suggest multiple orientations for the zeolitic H_2O molecules. The disorder also might reflect differences in the composition of the framework octahedra and tetrahedra, and/or the presence of extra octahedral cations in some of the tunnels. The major difference in the unit-cell parameters between the 100 K and RT structures is a decrease in *a* with cooling.

In situ heating of palygorskite

The synchrotron XRD data (Fig. 5) revealed a series of distinct phase changes as palygorskite (Korea) was heated in air to 1273 K, corresponding to a loss of zeolitic H_2O, sequential losses of structural H_2O molecules, and folding of the palygorskite structure after the structural H_2O(O4) was lost (Preisinger 1963; Hayashi et al. 1969). At the highest temperatures, an amorphous phase formed followed by the growth of β-quartz.

300 to 475 K—loss of zeolitic H_2O. During the temperature-resolved synchrotron XRD heating of palygorskite in air, the unit-cell volume decreased continuously by ~1.3% between ~345 and 425 K, reflecting a significant decrease in *a* and a slight increase in *b* (Fig. 6). Rietveld refinements using the XRD data indicated that most of the zeolitic H_2O was lost over this temperature range (Fig. 7). The β angle initially decreased, but at ~380 K it sharply increased, as seen in the first obvious phase change exhibited in the XRD patterns (Fig. 5). This transformation occurs at the loss of approximately one-half of the zeolitic H_2O from OW1 and OW2 (Fig. 7). Hayashi et al. (1969) observed the loss of zeolitic H_2O from palygorskite between 363 and 473 K using IR spectroscopy, and TGA measurements of palygorskite by Artioli et al. (1994) indicated that ~9% H_2O, equal to ~4 zeolitic H_2O molecules per eight tetrahedra, is lost between RT and 463 K. Giustetto and Chiari (2004) observed zeolitic H_2O loss in air from RT to ~425 K with a DTA peak at 383–393 K.

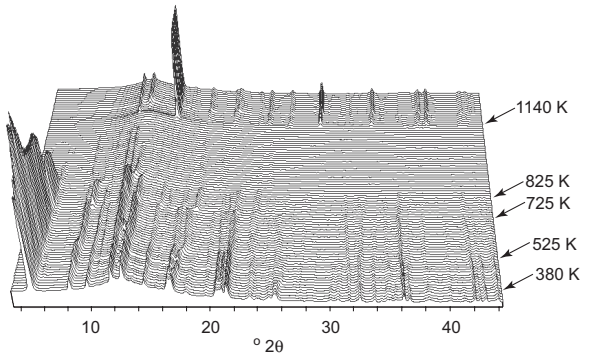

Figure 5. Synchrotron powder X-ray diffraction patterns for palygorskite (Korea) in air vs. temperature, from 300 (front pattern) to 1335 K.

The Rietveld refinements indicated that as palygorskite was heated, H_2O was lost at approximately the same rate from the two zeolitic H_2O sites. The occupancy factor refinements suggested that small amounts of H_2O remained on the sites to near 475 K. These small residual occupancies might be artifacts resulting from correlations among the occupancy factors, background coefficients and thermal factors during the least-squares refinements. The TGA studies mentioned above, however, showed that zeolitic H_2O loss might continue to ~463–473 K. Because OW2 probably forms H-bonds with O4 and O7, some H_2O molecules might linger at this site to higher temperatures. On the other hand, the chemical analyses for our palygorskite samples yielded slight excesses of octahedral cations. As discussed above, these excess cations might reside in the mostly vacant M1 site, but it is also possible that some or all of them are located in the tunnels, at the residual OW2 site. This interpretation is supported by the refined OW2 occupancy factor at 300 K that was slightly larger than expected for only O atoms (0.58 vs. 0.5).

Above 425 K, the palygorskite unit-cell volume was essentially unchanged to ~475 K (Fig. 6). Previous studies showed that for palygorskite samples heated to less than ~575 K, zeolitic H_2O is quickly replaced when samples are cooled to ambient temperature and humidity conditions (e.g., Preisinger 1963; Hayashi et al. 1969).

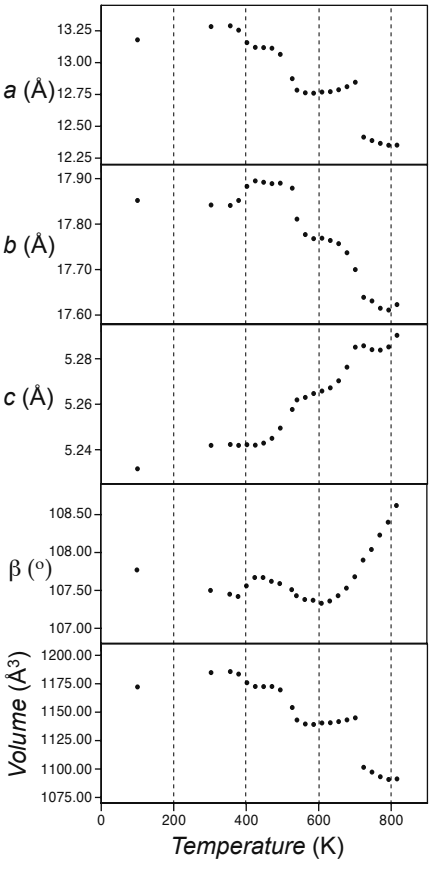

Figure 6. Plots of palygorskite unit-cell parameters vs. *T* for the range 300 to 815 K. The errors determined by the refinements are within the plotting symbols.

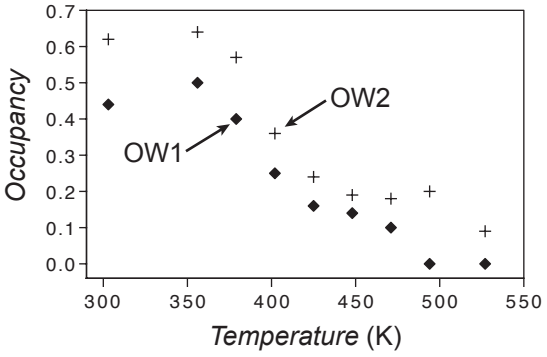

FIGURE 7. Plot of total number of zeolitic H_2O molecules determined by Rietveld refinements vs. *T*.

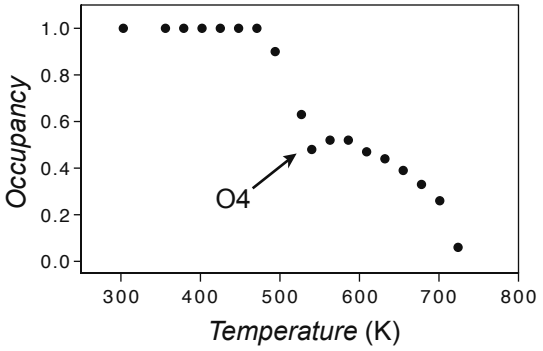

FIGURE 8. Plot of the refined occupancy factor for the bound H_2O(O4) in palygorskite vs. *T*.

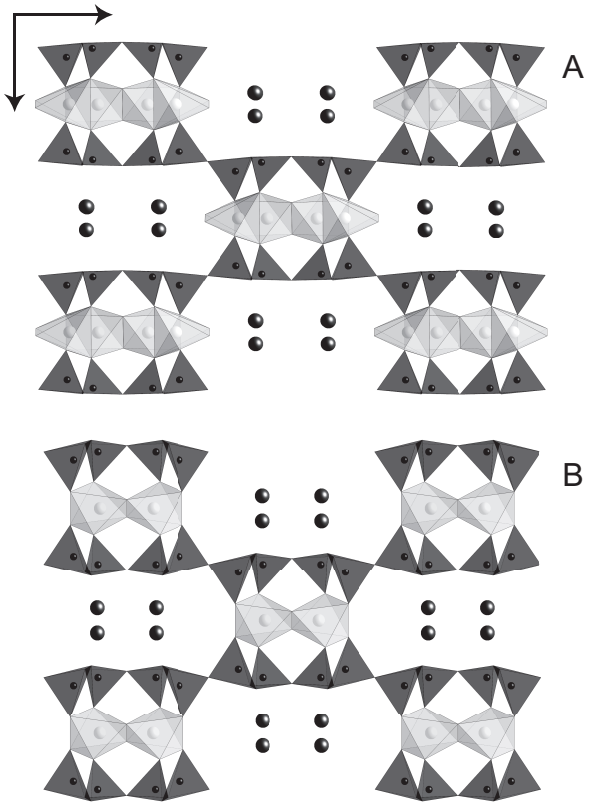

FIGURE 9. Polyhedral crystal structure representations, viewed along *c*, resulting from the Rietveld refinements for palygorskite (Korea) in air at 701 K (**a**) and 770 K (**b**). Shaded circles represent tunnel cations/anions.

475 to 725 K—loss of structural H_2O. The refined O4 occupancy factors (Fig.8) show that one-half (2 out of 4) of the structural H_2O was released between ~475 and 540 K. This H_2O loss coincided with a phase transition, at ~525 K, (Fig. 5), and resulted in a decrease in unit-cell volume of 2.9% (Fig. 6). Hayashi et al. (1969) similarly concluded from TGA experiments that the low temperature structural H_2O loss occurred between 483 and 623 K, and Artioli et al. (1994) reported a range of 453 to 573 from their TGA/DTG study. The *a* and *b* parameters decreased by 2.7% and 0.7%, respectively, whereas *c* increased 0.4% and the β angle decreased 0.3% (Fig. 6). Most of the change involves an inward bowing of the tunnels along *a*, and it occurs when about one-quarter of the total bound H_2O has exited the structure. With an occupancy factor of 0.5 H_2O molecules for O4, only one of the two O4 sites near each Mg is occupied, and the Mg is 5-coordinated. This is consistent with results of a Mössbauer study by Heller-Kallai and Rozenson (1981), who concluded that any Fe^{3+} in M3 became 5-coordinate upon heating.

The remaining two structural H_2O molecules were lost as palygorskite was heated from ~580 to 725 K (Fig. 8), and the XRD data showed a phase transition (Fig. 5). Previous TGA studies yielded similar temperature ranges for the higher-temperature water loss—523 to 773 K in Artioli et al. (1994) and 623 to 800 K in Hayashi et al. (1969). There was an abrupt decrease in volume (3.8%) coincident with this transition, associated with an equally sharp shortening of *a* (3.4%) (Fig. 6). Comparison of the refined palygorskite structures below and above the transition temperature (Fig. 9) reveals a dramatic inward buckling of the tunnels, consistent with the shortening of *a*, almost certainly a consequence of the loss of the structural H_2O. Also during this temperature interval, *b* declined 0.7%, *c* increased 0.4%, and the β angle increased from 107.4 to 107.9°. As the second half of the structural H_2O was lost, the O4 sites gradually merged to a single position.

The heating experiment showed that the structural H_2O is lost in two stages, with the loss of the first half occurring more quickly than the second half, over temperature intervals of 75 and 140°, respectively. This confirms similar observations made by Hayashi et al. (1969) from TGA experiments. They concluded that the second water loss is slowed by the folding of the structure, but as is discussed below, our heating experiment shows that all of the structural H_2O is lost almost 100 K below the temperature corresponding to the appearance of a folded structure. We did observe, however, a buckling of the framework that diminished the sizes of the tunnels when most of the second portion of structural H_2O had exited the structure.

Above ~600 K, the difference Fourier maps showed an area of increasing electron density in the tunnels near the lower temperature OW2 position. The refined occupancy factor increased to the equivalent of ~1.0 O atoms at ~725 K, and the site gradu-

ally moved toward the centers of the tunnels with increasing temperature. We observed a small occupancy factor (0.09) for OW2 even after all of the zeolitic H_2O apparently exited the structure, which likely accounts for some of this observed electron density. The increase in occupancy correlates well with the loss of the second half of the structural H_2O, and therefore might be related in part to movement of some of the H_2O to the center of the tunnels. Interestingly, our refinements also showed over this same temperature range a decrease in the Mg occupancy factor from 1 to ~0.20 and for O1 (OH) from 1 to 0.48, suggesting that some of the Mg and O1 atoms might be moving to the centers of the tunnels with increasing temperature. This interpretation is supported by the OW2 distance, which is close (2.0–2.10 Å) to the nearest framework O atom (O7), and this is a reasonable Mg-O bond length. Refinements of occupancy factors for other framework atoms showed no significant departures from 1.0. Apparently the movement of the Mg cations and the start of the loss of OH contribute to, or are a consequence of, the sharp buckling of the structure at 725 K (Fig. 9).

725 to 1273 K. The powder XRD patterns in Figure 5 show a folded palygorskite structure at ~655 K, as indicated by the diminishing of the intensity of the 10.5 Å basal reflection and rise of weak diffraction peaks at ~9.0 Å (~5 °2θ in Fig. 5). By ~825 K, most of the palygorskite structure decomposed, although a weak basal reflection persisted to ~990 K. The weak diffraction pattern for the folded palygorskite structure (Fig. 5) and the corresponding increase in the background indicate that for the Korean palygorskite heated in air only a small fraction of the sample folded, at least in an ordered way, and the remainder formed an amorphous phase. This differs from a similar study for sepiolite (Post et al. 2007) that showed the entire sample folded after the loss of the first half of the structural H_2O.

Compared to its close structural cousin sepiolite, palygorskite does not form a folded structure as easily. Also unlike sepiolite, which folded before all of the structural H_2O was lost, the transformation of palygorskite to a folded phase and an amorphous phase did not occur until ~100° above the departure of all of the bound H_2O. This more sluggish folding behavior may be attributed to the fact that the phyllosilicate ribbons in sepiolite are three silicate chains wide but only two in palygorskite, and the narrower ribbons build a less flexible structure. Additionally, the smaller Al, compared to Mg, in approximately one-half of the filled octahedral sites in palygorskite involves a reduction in the size of the octahedral sheet, which might make the structure more rigid. Perhaps also the migration of the Mg cations and O anions to the centers of the tunnels serves to prop open the tunnels and inhibit folding. Alaskan palygorskite heated in vacuum exhibited a stronger diffraction pattern for its folded configuration, along with an amorphous background. Structural collapse possibly is facilitated by the vacuum. Zeolitic and structural H_2O loss also occurred at significantly lower temperatures when samples were heated under vacuum, and palygorskite started folding at ~575 K.

Because of its more intense diffraction pattern, the modeling and Rietveld refinement of folded palygorskite was performed for the Alaskan sample that was heated in vacuum. The final refined model also fit well the diffraction pattern for the folded configuration in the Korean sample. The model for folded palygorskite agrees closely with the schematic model proposed by Preisinger (1963). Presumably, loss of the structural H_2O causes the palygorskite phyllosilicate ribbons to rotate, or fold, thereby reducing the cross-sectional area of the tunnels and changing the structure symmetry from $C2/m$ to $P2_1/a$. The unit-cell parameters for folded palygorskite at 1160 K are listed in Table 2 and differ slightly from those proposed by Preisinger (1963). The major departure is the β angle of 96.45° rather than ~90°.

Loss of structural H_2O requires Mg to complete its octahedral coordination in folded palygorskite by forming bonds, albeit long ones (~3.0 Å), to tetrahedral O atoms (O7) (Fig. 2). The Si-O and M-O bond constraints used in the refinements, however, might prevent adjustments that could result in a shorter Mg-O7 distance. Indeed, the need to complete the Mg coordination octahedron after the loss of the structural (O4) H_2O molecules might be the driving force causing the palygorskite structure to fold in conjunction with the absence of O4 H_2O molecules to prop open the tunnels. On the other hand, Guggenheim and Zhan (1999) showed that Mg can become a 3-coordinated ion in chlorite at high temperatures because of anion movement in the interlayer where space is available, and they suggest that Mg coordination at elevated temperatures when associated with tunnel edges (where space is available) might not require sixfold coordination. Refinement of the occupancy factor for O1 (OH) resulted in a value not significantly different from zero, indicating that the OH was lost prior to, or during, the folding of the structure, as is consistent with the heating of the Korean sample. Refinement of occupancy factors for other framework atoms did not yield values significantly different from 1.0, except for O8, which was ~0.3. Because of correlations among the occupancy factors for O7, O8, O7b, and O8b, and the decreased O8 occupancy was equally well described by a low occupancy factor in any one of these sites. Difference Fourier maps revealed an electron density peak near the center of the tunnel of the folded structure; an O atom (O9) added at that position refined to an occupancy factor 0f ~1.0. One interpretation of these results is that the tunnel site might contain O atoms either from the O7, O8 sites, or from the portion of the palygorskite sample that did not fold. These added O atoms might charge compensate for lost OH anions. The distances of the tunnel site to the surrounding O atoms range from 2.5 to 2.8 Å, which are appropriate for O-O bonds.

Hayashi et al. (1969) observed folded palygorskite after heating to ~625 K, a temperature 200 K lower than our experiments for the Korean palygorskite in air, although only above ~875 K was the transformation to folded palygorskite complete. Differences in transition temperature may be attributed to several factors: (1) Hayashi et al. examined a more Mg-rich palygorskite sample (Mg/Al =1.17 vs. 0.99 for our Korean sample); (2) they heated the sample for an hour, cooled it, and then collected powder XRD patterns; and (3) their sample was a mixture of monoclinic and orthorhombic palygorskite, and the polymorphs might behave differently. Heller-Kallai and Rozeson (1981) reported folding at 775 K, but some unfolded palygorskite remained until 875 K. They also noted that different palygorskite samples behave differently when heated. Similarly, Serna et al. (1975) note that the temperature ranges of the phase transitions in sepiolite are dependent on experimental conditions, such as the heating rate or whether the sample was

heated in air or vacuum. Nonetheless, the transition temperature range observed in our study is consistent with those reported by previous researchers.

Above ~960 K, the diffraction patterns for the Korean sample show no evidence of the folded structure but are consistent with an amorphous phase; there was no evidence of direct transformation of folded palygorskite to clinoenstatite as was observed by Preisinger (1963) and others. Preisinger (1963) suggested, however, that the formation and stability of clinoenstatite is a function of the Mg:Al ratio; for Mg:Al > 1, clinoenstatite is stable to 1273 K, but for Mg:Al < 1 the stability range is small. For both samples used in this study, Mg:Al <1, perhaps explaining why clinoenstatite did not form as the folded palygorskite decomposed. At ~1015 K, β-quartz diffraction peaks were detected and increased in intensity as heating continued to 1500 K. Cristobalite formed above ~1050 K, along with a small amount of clinoenstatite, and both phases persisted to the maximum temperature. Kulbicki (1959) heated palygorskite from Attapulgus, Georgia and observed the formation of clinoenstatite above 1073 K and β-quartz above 1373 K, both of which transformed to β-cristobalite above 1473 K. The formation and large stability range for clinoenstatite is consistent with Attapulgus palygorskites being more Mg-rich than the samples studied here.

Acknowledgments

Funding for this research was provided by NSF grants EAR01-25908 and EAR04-17741 and by a Penn State Materials Research Institute (MRI) SEED grant. We thank Jonathan Hanson of the Brookhaven National Lab for his assistance with the diffraction experiments at beamline X7B at the NSLS. This research was performed at the National Synchrotron Light Source, Brookhaven National Laboratory, which is supported by the U.S. Department of Energy, Division of Materials Sciences and Division of Chemical Sciences, under contract no. DE-AC02-98CH10886. The manuscript was significantly improved by the expert and thorough review provided by Stephen Guggenheim, and by the efforts of Associate Editor Przemyslaw Dera

References cited

Artioli, G., Galli, E., Burattini, E., Cappuccio, G., and Simeoni, S. (1994) Palygorskite from Bolca, Italy: A characterization by high-resolution synchrotron radiation powder diffraction and computer modeling. Neues Jahrbüch für Mineralogie Monshaft, 271–229.

Bradley, W.F. (1940) The structural scheme of attapulgite. American Mineralogist, 25, 405–410.

Brown, G.E., Sueno, S., and Prewitt, C.T. (1973) A new single-crystal heater for the precession camera and four-circle diffractometer. American Mineralogist, 58, 698–704.

Cámara, F., Garvie, L.A.J., Devouard, B., Groy, T.L., and Buseck, P.R. (2002) The structure of Mn-rich tuperssuatsiaite: a palygorskite-related mineral. American Mineralogist, 87, 1458–1463.

Chiari, G., Giustetto, R., and Ricchiardi, G. (2003) Crystal structure refinements of palygorskite and Maya Blue from molecular modeling and powder synchrotron diffraction. European Journal of Mineralogy, 15, 21–33.

Chisholm, J.E. (1992) Powder diffraction patterns and structural models for palygorskite. Canadian Mineralogist, 30, 61–73.

Christ, C.L., Hathaway, J.C., Hostetler, P.B., and Shepard, A.O. (1969) Palygorskite: New X-ray data. American Mineralogist, 54, 198–205.

Corma, A., Mifsud, A., and Sanz, E. (1990) Kinetics of the acid leaching of palygorskite: Influence of the octahedral sheet composition. Clay Minerals, 25, 197–205.

De Lapparent, J. (1935) Sur un constituent essential des terres a foulon. C.R. Academie Science, Paris, 203, 482.

Drits, V.A. and Sokolova, G.V. (1971) Structure of palygorskite. Soviet Physics—Crystallography, 16, 183–185.

Finger, L.W., Cox, D.E., and Jephcoat, A.P. (1994) A correction for powder diffraction peak asymmetry due to axial divergence. Journal of Applied Crystallography, 27, 892–900.

Fois, E., Gamba, A., and Tilocca, A. (2003) On the unusual stability of Maya blue paint: molecular dynamics simulations. Microporous and Mesoporous Materials, 57, 263–272.

Galan, E. (1996) Properties and applications of palygorskite-sepiolite clays. Clay Minerals, 31, 443–453.

Galan, E. and Carretero, M.I. (1999) A new approach to compositional limits for sepiolite and palygorskite. Clays and Clay Minerals, 47, 399–409.

Giustetto, R. and Chiari, G. (2004) Crystal structure refinement of palygorskite from neutron powder diffraction. European Journal of Mineralogy, 16, 521–532.

Guggenheim, S. and Zhan, W. (1999) Crystal structures of two partially dehydrated chlorites: The "modified" chlorite structure. American Mineralogist, 84, 1415–1421.

Güven, N., de la Caillerie, J., and Fripiat, J.J. (1992) The coordination of aluminum ions in the palygorskite structure. Clays and Clay Minerals, 40, 457–461.

Hammersley, A.P., Svensson, S.O., Hanfland, M., Fitch, A.N., and Hausermann, D. (1996) Two-dimensional detector software: From real detector to idealized image or two-theta scan. High Pressure Research, 14, 235–248.

Hayashi, H., Otsuka, R., and Imai, N. (1969) Infrared study of sepiolite and palygorskite on heating. American Mineralogist, 53, 1613–1624.

Heller-Kallai, L. and Rozenson, I. (1981) Mössbauer studies of palygorskite and some aspects of palygorskite mineralogy. Clays and Clay Minerals, 29, 226–232.

Jones, B.F. and Galan, E. (1988) Sepiolite and palygorskite. In S.W. Bailey, Ed., Hydrous Phyllosilicates, 19, p. 631–674. Reviews in Mineralogy, Mineralogical Society of America, Chantilly, Virginia.

José-Yacamán, M., Rendón, L., Arenas, J., and Serra Puche, M.C. (1996) Maya Blue paint: An ancient nanostructured material. Science, 273, 223–225.

Kuang, W., Facey, G.A., and Detellier, C. (2004) Dehydration and rehydration of palygorskite and the influence of water on the nanopores. Clays and Clay Minerals, 52, 635–642.

Kulbicki, G. (1959) High temperature phases in sepiolite, attapulgite, and saponite. American Mineralogist, 44, 752–764.

Larson, A.C. and Von Dreele, R.B. (2007) GSAS-General Structure Analysis System. Los Alamos National Laboratory Report No. LAUR 86–748.

Pluth, J., Smith, J., Pushcharovskii, D.Y., Semenov, E.I., Bram, A., Riekel, C., Weber, H., and Broach, R.W. (1997) Third-generation synchrotron X-ray diffraction of 6-μm crystal of raite, $\approx Na_3Mn_3Ti_{0.25}Si_8O_{20}(OH)_2 \cdot 10H_2O$, opens up new chemistry and physics of low-temperature minerals. Proceedings of the National Academy of Sciences, U.S.A., 94, 12263–12267.

Post, J.E. and Bish, D.L. (1989) Rietveld refinement of crystal structures using powder X-ray diffraction data. In D.L. Bish and J.E. Post, Eds., Modern Powder Diffraction, 20, p. 277–308. Reviews in Mineralogy, Mineralogical Society of America, Chantilly, Virginia.

Post, J.E., Bish, D.L., and Heaney, P.J. (2007) Synchrotron powder X-ray diffraction study of the structure and dehydration behavior of sepiolite. American Mineralogist, 92, 91–97.

Preisinger, A. (1963) Sepiolite and related compounds: its stability and application. Clays and Clay Minerals, 10, 365–371.

Rautureau, M. and Mifsud, A. (1977) Etude par microscope electronique des differents etats d'hydration de la sepiolite. Clay Minerals, 12, 309–318.

Serna, C., Ahlrichs, J.L., and Serratosa, J.M. (1975) Folding in sepiolite crystals. Clays and Clay Minerals, 23, 452–457.

Serna, C., VanScoyoc, G.E., and Ahlrichs, J.L. (1977) Hydroxyl groups and water in palygorskite. American Mineralogist, 62, 784–792.

Shannon, R.D. (1976) Revised effective ionic radii and systematic studies of interatomic distances in halides and chalcogenides. Acta Crystallographica, A32, 751–767.

Smith, D.G.W. and Norem, D. (1986) The electron microprobe analysis of palygorskite. Canadian Mineralogist, 24, 499–511.

Stephen, I. (1954) An occurrence of palygorskite in the Shetland Isles. Mineralogical Magazine, 30, 471–480.

Stephens, P.W. (1999) Phenomenological model of anisotropic peak broadening in powder diffraction. Journal of Applied Crystallography, 32, 281–289.

Thompson, P., Cox, D.E., and Hastings, J.B. (1987) Rietveld refinement of Debye-Scherrer synchrotron X-ray data from Al_2O_3. Journal of Applied Crystallography, 20, 79–83.

Tien, P. (1973) Palygorskite from Warren Quarry, Enderby, Leicestershire, England. Clay Minerals, 10, 27–34.

Van Scoyoc, G.E., Serna, C., and Ahlrichs, J.L. (1979) Structural changes in palygorskite during dehydration and dehydroxylation. American Mineralogist, 64, 216–223.

Manuscript received January 2, 2007
Manuscript accepted November 12, 2007
Manuscript handled by Przemyslaw Dera